FLYING V DIRECTIONAL FLIGHT CONTROL: AN EXPERIMENTAL INVESTIGATION

Roelof Vos[1], Nelson Johnson[1] & Stijn Nolet[1]

[1]Delft University of Technology

Abstract

The Flying V is a flying-wing aircraft where passengers, cargo, and fuel reside within the wing. In this study, two types of directional control surfaces are studied: rudders on the winglets and drag rudders on the outer wing. Wind tunnel testing on a 4.6% half-wing model of the Flying V is performed in the open-jet wind tunnel of TU Delft. Forces and moments are recorded using a balance at the model's base. It is shown that at zero angle of attack, the winglet rudders can induce a maximum yawing moment coefficient of 0.0065, while the drag rudders can only attain 0.0043. However, at a 25-degree angle of attack, the winglet rudders have a 70% reduction in effectiveness, while the drag rudders have only reduced by 20%. A superposition of the winglet rudders and a 5%-span drag rudder shows that a yawing moment of 0.0045 can be ensured up to a 30-degree angle of attack. It is therefore concluded that future design iterations of the Flying V should use winglet rudders combined with drag rudders to ensure adequate directional control over the entire flight envelope.

Keywords: flying wing, control surface, wind tunnel testing, rudder, directional control

Nomenclature

Latin Symbols

b	span [m]
C_D	drag coefficient [-]
C_L	lift coefficient [-]
C_D	drag coefficient [-]
C_n	yawing moment coefficient [-]
$l,\ m,\ ,n$	rolling, yawing, pitching moment [Nm]
S	wing area [m^2]
V	velocity [m/s]
$x,\ y,\ z$	coordinates [m]

Greek Symbols

α	angle of attack [deg]
δ	deflection angle [deg]
ρ	density [kg/m^3]

Subscripts

a	aerodynamic
b	body
dr	drag rudder
r	rudder
ref	reference
wr	winglet rudder

Acronyms

CS	control surface
OJF	open jet facility
VLM	vortex lattice method
WL	winglet

1 Introduction

The Flying V is a flying-wing aircraft that houses the passengers, freight, and fuel inside the wing. It has two over-the-wing turbofan engines for propulsion and winglets that double as vertical tailplanes. An artist's impression of the Flying V is shown in Figure 1. For primary flight control, the Flying V has simple control surfaces mounted on the outboard wing and the winglet. They act as elevons and rudders, respectively. Due to a lower wetted area, a spanwise distribution of weight, and an increased effective span, the Flying V requires 20% less energy than a comparable tube-and-wing aircraft [1]. An overview of the Flying V research and design efforts of the Flying V can be found in Ref. [2].

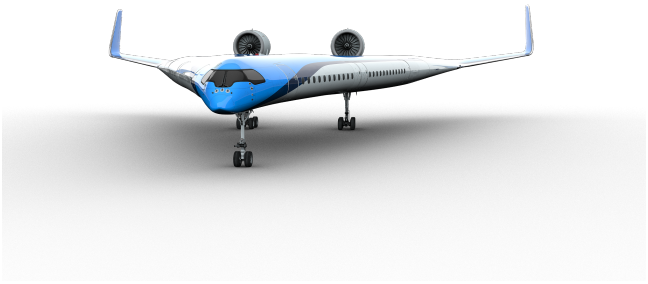

Figure 1 – Artist's impression of the Flying V long-haul passenger aircraft.

The handling qualities of the Flying V have been experimentally investigated in the SIMONA flight simulator of TU Delft [3]. Based on these tests, it was found that the Flying V lacks lateral-directional control power and control power at landing conditions, mainly when the center of gravity is at its most forward location. The aerodynamic model that the authors of Ref. [3] used to perform their analysis and experiments was created by Cappuyns [4]. He used a vortex-lattice method (VLM) to predict the control effectiveness of the control surfaces on the outboard wing and the winglet. Since the VLM method is expected to over-predict control-surface effectiveness, it is clear that the lateral-directional control properties need to be further improved to ensure adequate handling qualities of the Flying V.

To that end, this paper presents an experimental investigation into the effect of the directional control authority. First, the effectiveness of the winglet rudder is experimentally characterized. Secondly, drag rudders are introduced on the outboard wing. Most fielded flying-wing aircraft rely on drag rudders for directional control, e.g., XB-35, B-2, and the B-21 Raider. It is hypothesized that drag rudders can improve directional control substantially, particularly at high angles of attack. In this paper, this hypothesis is tested through an experimental investigation in the wind tunnel.

The paper is structured as follows. In Section 2, we present the experimental method used to quantify the aerodynamic coefficients. The experimental setup for the winglet rudder and the drag rudder are described. Section 3 compares the experimental results to previous wind tunnel experiments to validate the result. In Section 4, we present the experimental results. Section 5 presents the conclusions of this research.

2 Methodology

An experimental approach is followed to determine the effect of the proposed control surfaces. A 4.6%-scale half-wing model of the Flying V is used. Palermo and Vos describe this model in Ref. [5]. The model measures 1.5 meters in span, is made out of glass fiber, and is mounted on a force balance connected to a turn table. The wing is positioned in the Open Jet Facility of TU Delft, a closed-loop, low-speed, open-test-section wind tunnel facility with a maximum attainable flow velocity of 35 m/s. A drawing of the wind tunnel setup is shown in Figure 2.

The test article features a winglet measuring 0.35 m in height, having a leading-edge sweep angle of 36°, an aspect ratio of 3, a taper ratio of 0.6, and a NACA 0018 airfoil. This results in an 45% larger winglet compared to the one that Cappuyns [4] used for this study. In addition, three control surfaces are present on the wing's trailing edge. Their dimensions are described in Ref. [5]. In the present study, these control surfaces are not deflected, although the most outboard control surface is used to mount the drag rudders.

Figure 3 shows the body-fixed (subscript b) and aerodynamic (subscript a) reference frames. The body-fixed reference frame is rotated by angle-of-attack α over the y-axis. As we only consider symmetric conditions, the y-axis of the body reference frame and the aerodynamic reference frame are the same. The yawing moment, n, is measured with respect to the vertical axis of the body reference frame, z_b. A positive deflection of the winglet rudder on the port-side wing means the rudder deflects outboard. This causes a negative yawing moment. A positive deflection of the drag

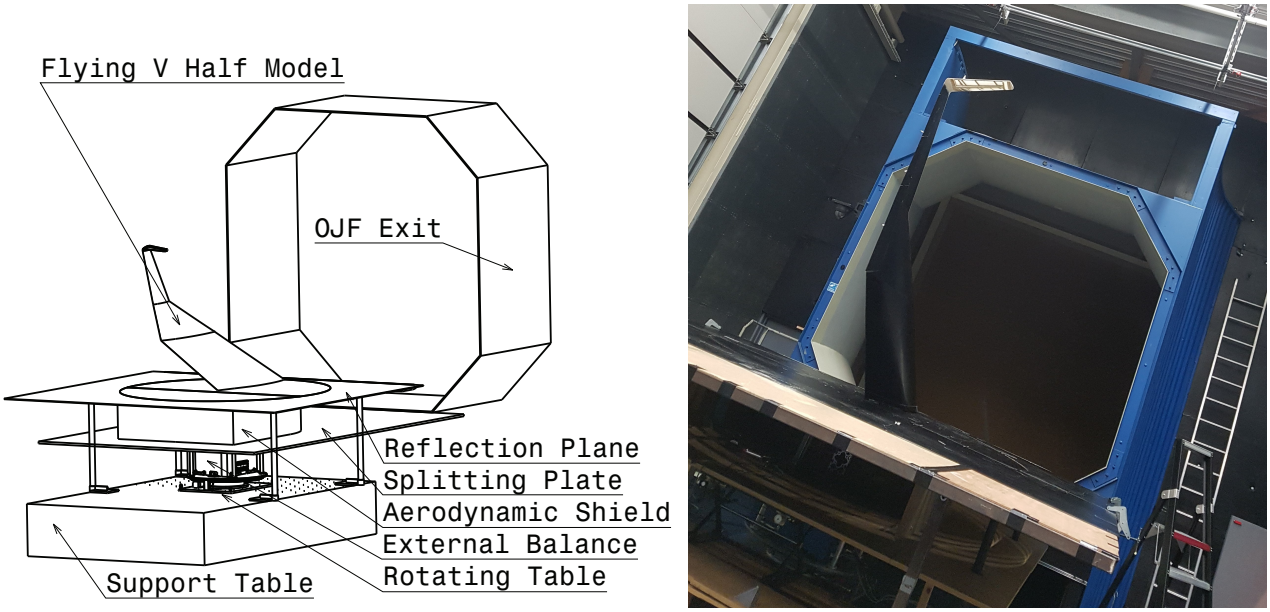

Figure 2 – Flying V half model in the Open Jet Facility (OJF) of TU Delft. Schematic (left) and photograph (right). The span of the half model is 1.5m. This drawing and image previously appeared in Ref. [6].

rudder on the port-side wing also produces a negative yawing moment. Therefore, both yawing moment derivatives with respect to deflection are negative.

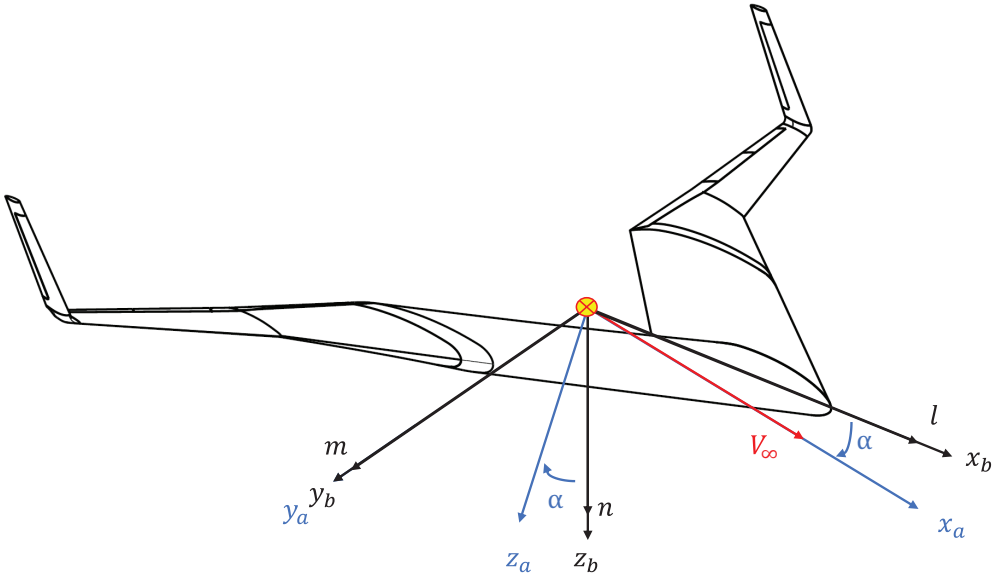

Figure 3 – Body-fixed and aerodynamic reference frames for zero sideslip. The rolling, pitching, and yawing moments are indicated with l, m, and n, respectively. This image previously appeared in Ref. [6].

To compute the yawing moment produced by the winglet rudders or one of the drag rudders, the following expression is used:

$$C_n = \frac{2\Delta n}{\rho V^2 S_{\text{ref}} b_{\text{ref}}} \tag{1}$$

where Δn is the change yawing moment induced by rudder deflection measured in Newtons, ρ is the air density in kg/m^3 derived from the measured temperature and pressure, $S_{\text{ref}} = 1.87$ m^2 is the reference area of the wing, and $b_{\text{ref}} = 2.99$ m is the reference span of the wing. Note that even when testing the rudder on a half-wing model of the Flying V, the coefficients are computed with the span

and reference area of the complete Flying V. The mean geometric chord measures 0.82 m and is used as the reference chord.

2.1 Winglet Rudders

The winglet has a rudder spanning the upper 90% of the trailing edge with a chord ratio of 0.3. The rudder features a horn balance at the tip extending to the winglet's leading edge and spans the last 15% of the winglet height. The maximum deflection of the rudder is 23 degrees in either direction. The rudder's leading edge is flat, causing an appreciable gap when deflecting. A front view and side view of the winglet and rudder are shown in Figure 4.

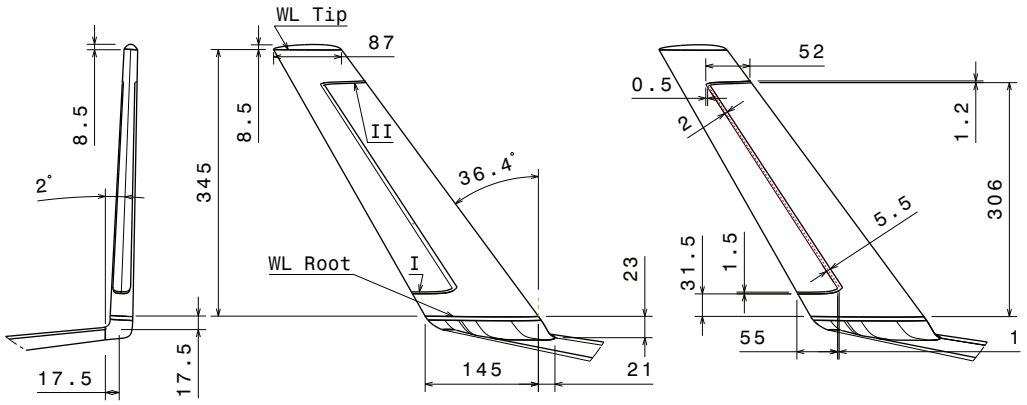

Figure 4 – Dimensions of the winglet (WL) and rudder [6]

2.2 Drag Rudders

The port-side semi-wing of the Flying V has three control surfaces (CS) marked 1 through 3 from inboard to outboard. In this experiment, drag rudders are assumed to replace (part of) the most outboard control surface of the test article. Figure 5 shows that four drag rudder sizes are proposed, ranging from 10 cm to 22 cm in span. The cross-sectional view, BB' shows how the drag rudder deflection is measured. The notional hinge line of each panel is located at the thickest point of the outboard control surface. The maximum deflection achieved by each drag rudder is 60 degrees. The drag rudders are held in position by 3D-printed brackets.

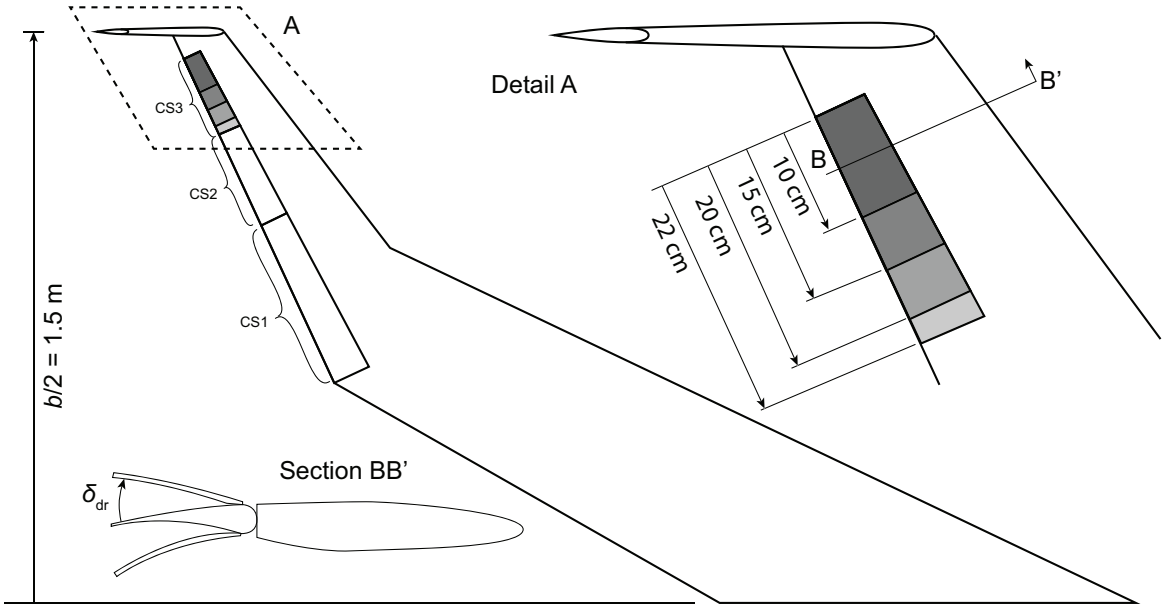

Figure 5 – Design of the drag rudders on the port-side wing. The most outboard control surface (CS3) mounts four drag rudders of various lengths. Modified from Ref. [6].

A picture of the outer wing is shown in Figure 6. Here, the wing is experiencing a 20 m/s flow velocity and is at an angle of attack of 15 degrees. A drag rudder of 15 cm (5% of the span) is positioned over the outboard wing with a symmetric deflection of $\delta_{\text{dr}} = 40^\circ$. The tufts indicate a strong outboard flow of the boundary layer over most of the outer wing. Only near the winglet can we see the tufts aligning more to the freestream direction.

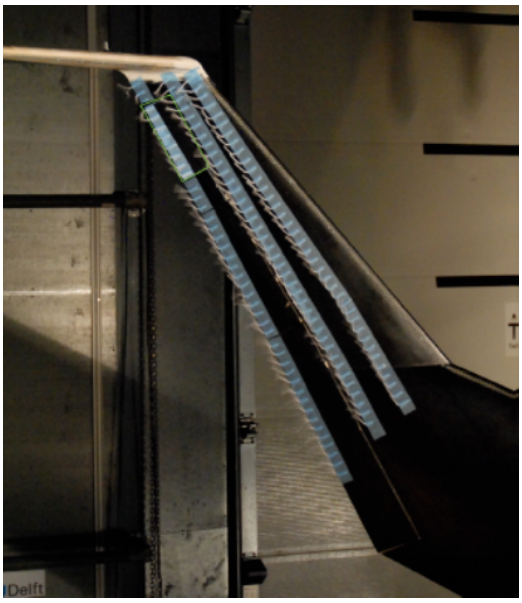

Figure 6 – Experimental setup with 40-degree deflection of upper drag-rudder panel and tufts. Photo: S. Nolet from Ref. [7].

3 Validation

The experimental data presented in this paper has been obtained throughout four wind tunnel campaigns. In this section, it is shown how the obtained results compare to previous experiments performed using the same test article, wind tunnel, and setup. Secondly, the repeatability of the experiment is demonstrated by comparing the results from the four campaigns.

Previous experiments that used the experimental setup of Section 2 are documented in References [5, 8, 9, 10]. Here, Ref. [5] and Ref. [10] are used to compare the experiments to. In Ref. [5], Palermo and Vos report the experimental results of the starboard wing of the Flying V without a winglet. A trip strip in the form of zig-zag tape is present on the suction side of the wing at 5% of the local chord and on the pressure side of the wing at 10% of the local chord. They report a maximum measured lift coefficient of 1.02 at an angle of attack of 35 degrees and a pitch break at an angle of attack of 20 degrees resulting in a usable maximum lift coefficient of $C_L = 0.80$. Figure 7 shows the lift curve and drag polar of this experiment in purple. Owing to its large sweep angle and low aspect ratio, a lift curve slope of $C_{L_\alpha} = 1.9$ per radian for angles of attack below 10 degrees. At 10 degrees, a break in the lift curve can be observed, which is associated with the formation of vortices according to Ref. [11].

In Ref. [10], this experiment is repeated on the same wing without the application of the trip strips on either side of the wing. This results in a two-degree increase in the zero-lift angle of attack, as seen in the cyan curve on the left-hand side of Figure 7. Also, the kink in the lift curve is absent and the maximum lift coefficient is raised to 1.04. The pitch break is less pronounced, and only at $C_L = 0.95$ do we see a sustained positive gradient of the pitching moment with the angle of attack. The absence of the trip strip also reduced the friction drag, as can be clearly seen in the drag polar on the right-hand side of Figure 7. The minimum drag occurs at a lift coefficient $C_L = 0.15$, corresponding to $\alpha = 5^\circ$. It is concluded that the removal of the trip strip has favorable characteristics for the wind tunnel model and all subsequent tests are performed without trip strips.

In this study, four wind tunnel campaigns are performed labeled in Figure 7 as “Johnson 1,” “Johnson

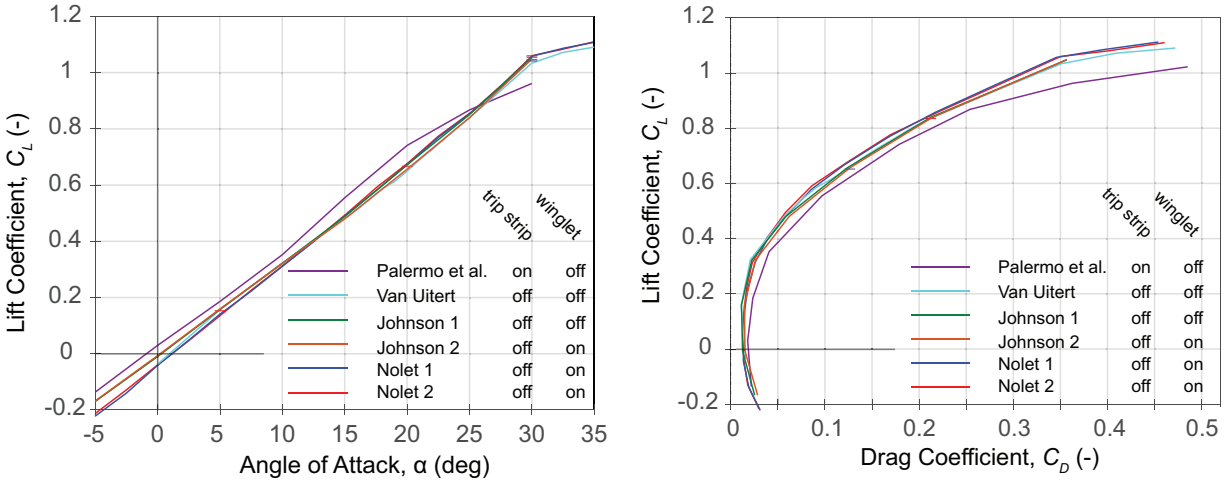

Figure 7 – Comparison of lift curve (left) and drag polar (right) results to previous studies. The Reynolds number is between 1.0 and 1.1 million for all experiments.

2," "Nolet 1," and "Nolet 2," after the author that lead each campaign. In the campaign labeled with "Johnson 1," exactly the same experiment as Van Uitert [10] is conducted. If we compare the lift curve, we see that the green line (Johnson 1) and the cyan line (Van Uitert) have the same slope and overall shape. The zero-lift angle of attack is approximately one degree smaller, which could be attributed to a slight misalignment of the setup in the wind tunnel. If we compare the drag polars of these two experiments, we can see that the lines are virtually on top of each other, which indicates that the experiment is properly repeated.

In "Johnson 2" the winglet is added. This corresponds to the brown lines in Figure 7. In the drag polar the addition of the winglet can be observed by a small increase in the minimum drag coefficient. This is expected as a result of the larger wetted area. At lift coefficients higher than 0,2, the winglet reduces the drag slightly, although the lines two campaigns by Johnson are still very close. Also in the lift curves, the difference between the green and the brown curve is almost negligible. This indicates that the winglet has very little effect on the lift and drag characteristics of the wing.

The two subsequent campaigns, marked with "Nolet 1" and "Nolet 2" are indeed a repetition of Johnson's second campaign in terms of geometry. For $\alpha > 12.5^\circ$ the lift curves of these three campaigns are almost the same. At smaller angles of attack, the lift is slightly reduced and the zero-lift angle of attack is again about 1 degree larger than for "Johnson 2." If we compare the drag polars, we can see that the curves for "Nolet 1" and "Nolet 2" are practically identical, indicating good repeatability. However, For $C_L > 0.3$ the drag polar shows that Nolet recorded consistently less drag than the second campaign of Johnson. These small differences are attributed to a slight misalignment between the two setups of Johnson and Nolet.

In conclusion, this validation study demonstrates that the measurements taken during the four wind tunnel campaigns can be trusted. The experiment is repeatable, yielding the same results. The effect of the trip strip is rather large on the lift and drag characteristics at this Reynolds number of 1 million. Since full-scale Reynolds numbers are two orders of magnitude higher, care must be taken when converting the results to full-scale conditions.

4 Results

In this section, the results of the four wind tunnel campaigns are presented. The focus is on the effect of the yawing moment coefficient. All other forces and moments are reported in Refs. [6] and [7]. We first discuss the effect of the deflection of the winglet rudder and the drag rudder on the yawing moment coefficient. Then, we present the rudder effectiveness of the winglet rudders and the drag rudders.

4.1 Yawing Moment Coefficient

The variation in yawing moment due to winglet rudder deflection of the port-side wing is shown in Figure 8. Each line in this graph represents a constant deflection angle of the port-side-wing winglet rudder. Deflection angles are varied between $\delta_{wr} = -23°$ and $\delta_{wr} = +23°$. The angle of attack varies between -5° and +30°.

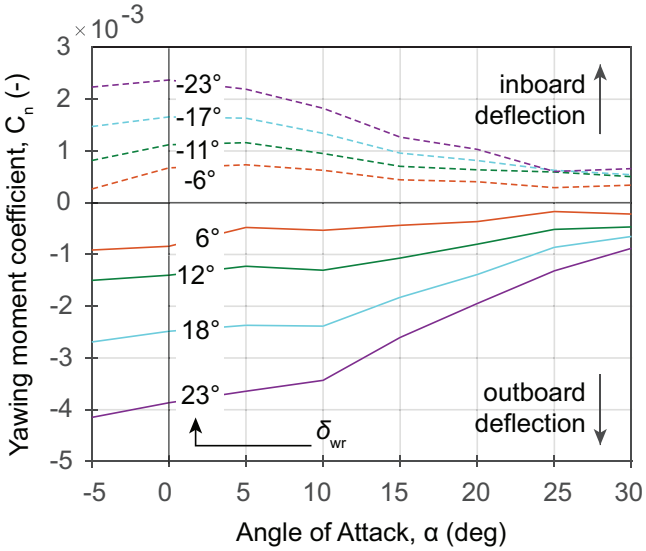

Figure 8 – Yawing moment variations with angle of attack for port-side-wing winglet rudder deflections ranging from -23 degrees to +23 degrees. Re $= 1.1 \cdot 10^6$

The graphs in Figure 8 show that the outboard deflection (positive values of δ_{wr}) of the winglet rudder results in a larger change in yawing moment compared to the inboard deflection of the rudder. At $\alpha = 0°$ and for maximum rudder deflection, the outboard deflection results in a 60% larger change in yawing moment compared to the inboard deflection. Secondly, it can be seen that rudder effectiveness declines dramatically with an increased angle of attack. At a 30-degree angle of attack, only 25% of the original rudder effectiveness is left. This is mainly attributed to the increase in the effective sweep angle of the hinge line, reducing the control surface effectiveness.

Three drag rudders measuring 10, 15, and 20 cm in span were tested. This is 3.3%, 5.0%, and 6.7% of the span, respectively. The tip of each drag rudder was located at 98% of the semi-span. Each of the drag rudders could be deflected up to 60 degrees.

On the left-hand side of Figure 9, the yawing moment due to both winglet rudders are combined. This gives a good indication of the aircraft's controllability at various angles of attack. First of all, it can be observed that the lines are fairly straight up to maximum deflection, indicating an almost linear response of the yawing moment with respect to rudder deflection. Secondly, one can see that the maximum absolute yawing moment achieved with these rudders is $C_n = 0.0065$. Finally, it can be observed that with an increased angle of attack, the slope of the control curve is reduced. This indicates that the rudder control power declines by about 75% between $\alpha = 0°$ and between $\alpha = 30°$.

On the right-hand side of Figure 9 it can be seen that the maximum negative yawing moment of the drag rudder amounts to -0.0039 at zero angle of attack and 60-degree deflection. This is 30% less than the maximum yawing moment generated by the winglet rudders at zero angle of attack. However, contrary to the winglet rudders, the drag rudders have a lower dependency on the angle of attack. For example, at 25 degrees, we still have a yawing moment of -0.0033, which is 60% more than the maximum yawing moment generated by the rudders (right-hand side of Figure 9). The drag rudders are, therefore, less sensitive to changes in angle of attack compared to the winglet rudders.

4.2 Rudder Effectiveness

For control purposes, it is relevant to quantify the yawing-moment-due-to-rudder deflection ($C_{n_{\delta r}}$) as a function of the angle of attack. A linear interpolation is applied to estimate this derivative for the two

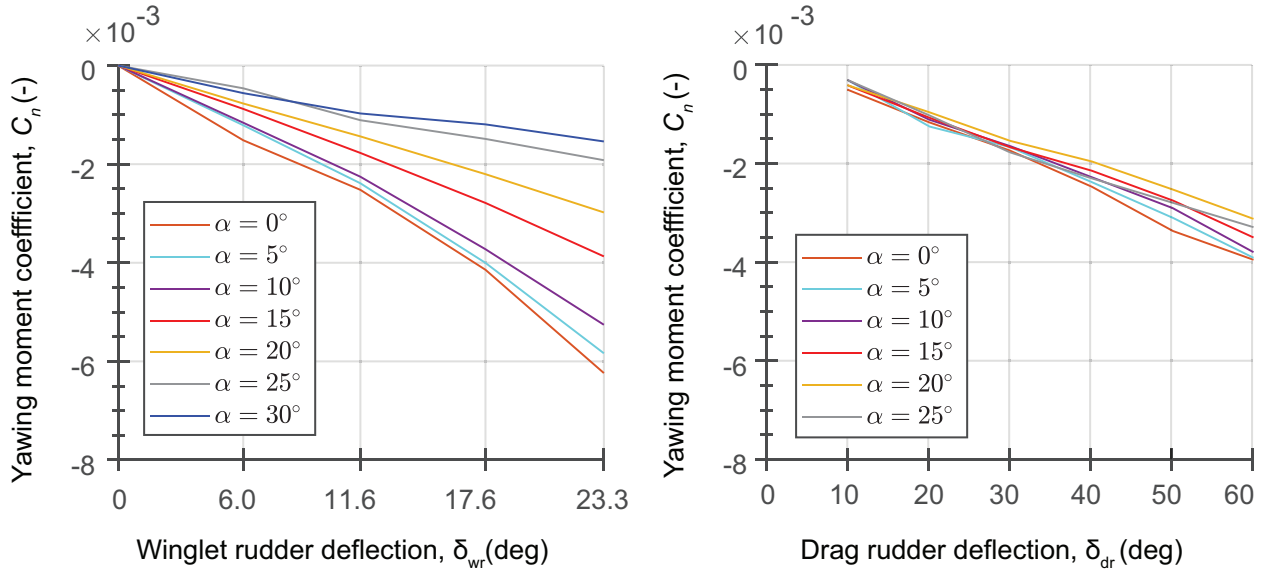

Figure 9 – Yawing moment coefficient due to deflection of both winglets (left) and due to deflection of a 5%-span drag rudder (right). Re $= 1.1 \cdot 10^6$

winglet rudders and the drag rudder. This coefficient is shown on the left-hand side of Figure 10.

If we compare the effectiveness of the winglet rudders and the drag rudder, we see that the winglet rudders produce a much larger change in yawing moment per radian of deflection compared to the drag rudder. However, the winglet rudders show a nonlinear decrease in effectiveness with the angle of attack. Up to 10 degrees, this decay with angle of attack is smaller than above 10 degrees. It was shown in previous work by Viet that the wing starts generating vortices at an angle of attack of approximately 10 degrees [Viet 2019]. Whether there is a connection between vortex formation and rudder effectiveness is unknown. The effectiveness of a 5%-span drag rudder also decreases slightly with angle of attack. However, this decay is much smaller compared to the winglet rudders. At $\alpha = 25°$, the drag rudders still have 80% of their effectiveness left.

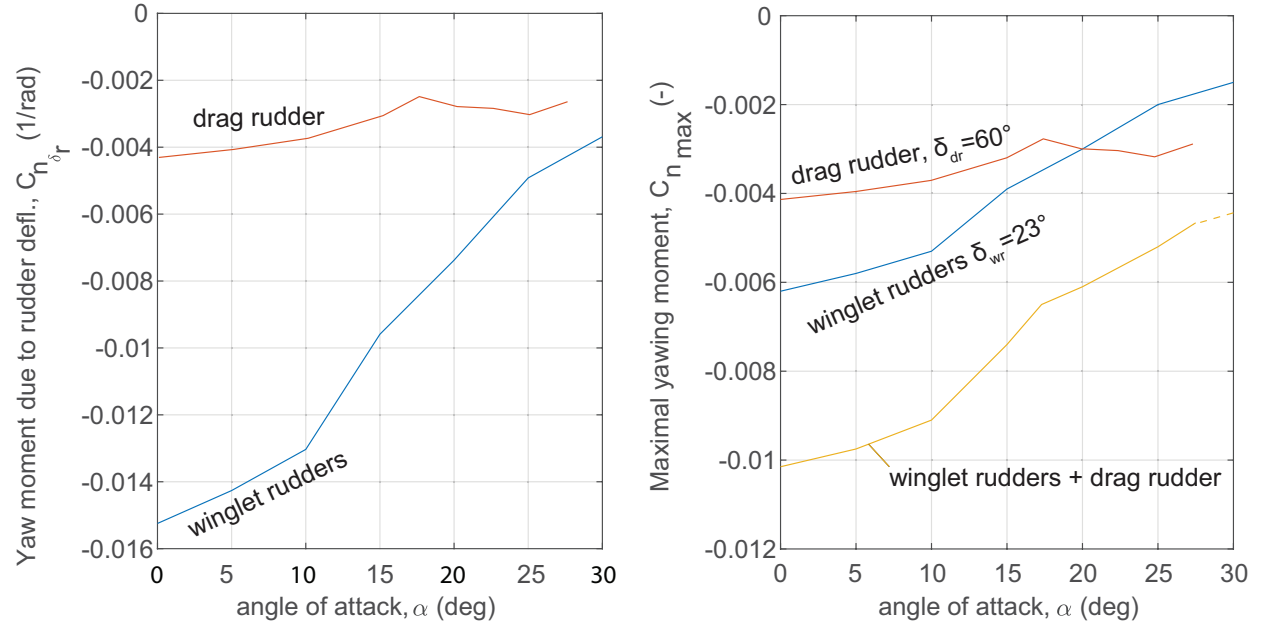

Figure 10 – Yawing moment derivative with rudder deflection (left) and yawing moment generated at maximal tested rudder deflection (right). Results for a 5%-span drag rudder. Re $= 1.1 \cdot 10^6$

On the right-hand side of Figure 10, the maximal yawing moment produced by the winglet rudders and the drag rudder are plotted, along with superposition of both lines. Because the drag rudders reach

a much higher maximal deflection than the winglet rudders, the disparity between the two yawing-moment curves is much smaller than would be expected based on their respective effectiveness curves (left-hand side of Figure 9). At an angle of attack of 20 degrees, the yawing moment of the two winglet rudders equals that of the single drag rudder. For all angles of attack above 20 degrees, the drag rudder can produce a higher yawing moment than the two winglet rudders combined. If we superimpose the two lines, it can observed that the combination of the two winglet rudders can ensure that up to 30-degree angle-of-attack, a yawing moment coefficient of -0.0045 can be produced.

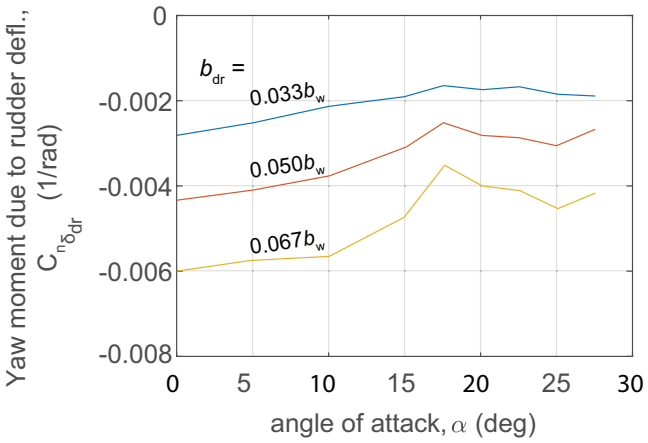

Figure 11 – Drag rudder effectiveness as a function of the drag rudder span (b_{dr}). Experimental results at Re $= 1.1 \cdot 10^6$. Drag rudders according to layout in Figure 5.

In Figure 11, the effectiveness of the drag rudder is plotted as a function of their wing span. While the previous paragraphs discussed the impact of a 5%-span drag rudder, here we also see the effect of a smaller (3.3%-span) and larger (6.7%-span) drag rudder. These three spans correspond to the 10-cm, 15-cm and 20-cm drag rudders shown in Figure 5. For angles of attack below 10 degrees, we can see that the span almost linearly increases the effectiveness. However, between $15^\circ < \alpha < 20^\circ$, we see that the 6.7% span drag rudder loses more effectiveness than the 5%-span drag rudder, which loses more effectiveness than the 3.3%-span drag rudder. It is hypothesized that this is caused by flow separation happening outboard of the leading-edge kink. However, this hypothesis is not tested in this study.

5 Conclusions

Winglet rudders and drag rudders are tested in the wind tunnel to determine their effect on the directional control power on a 4.6%-scale, half-wing test article of the Flying V at a Reynolds number of one million. A comparison with previous wind tunnel results shows that these experiments have excellent repeatability. Results show that the two winglet rudders can generate a maximum yawing moment coefficient of 0.0065 at zero angle of attack. In contrast, a 5%-span drag rudder yields a yawing moment coefficient of 0.0043. However, at a 25-degree angle of attack, the winglet rudders have a 70% reduction in control power, while the drag rudders only reduce by 20%. The drag rudders are shown to increase total directional control power by 150% at an angle of attack of 25 degrees. The superposition of a 5%-drag rudder and the two winglet rudders ensures that the yawing moment can remain above 0.0045 over the entire range of angles of attack. It is, therefore, concluded that future iterations of the Flying V should employ a combination of winglet rudders and drag rudders for adequate directional control.

6 Contact Author Email Address

Roelof Vos is contact author for this article. r.vos@tudelft.nl

7 Copyright Statement

References

[1] Wilco Oosterom and Roelof Vos. Conceptual design of a flying-v aircraft family. In *AIAA AVIATION 2022 Forum*.

[2] Justus Benad and Roelof Vos. Design of a flying v subsonic transport. In *Proceedings of the 33rd Congress of the International Council of the Aeronautical Sciences (ICAS 2022)*, pages 358–365, Stockholm, Sweden, September 4-9 2022. ICAS.

[3] Joosten, S, Stroosma, O., Vos, R., and Mulder, M. Simulator assessment of the lateral-directional handling qualities of the flying-v. In *AIAA SciTech Forum*, 2023.

[4] T. Cappuyns. Handling Qualities of a Flying V Configuration. Master's thesis, Delft University of Technology, 2019.

[5] Palermo, P., and Vos, R. Experimental aerodynamic analysis of a 4.6%-scale flying-v subsonic transport. In *AIAA SciTech Forum*, 2020.

[6] Nelson Johnson. Effect of winglet integration and rudder deflection on flying-v aerodynamic characteristics. Master's thesis, Delft University of Technology, Delft, The Netherlands, 2021.

[7] Stijn Nolet. Improving the flying v directional control power by the implementation of split flapss. Master's thesis, Delft University of Technology, Delft, The Netherlands, 2022.

[8] Ruiz Garcia, A., Vos, R., and De Visser, C. C. Aerodynamic model identification of the flying v from wind tunnel data. In *AIAA Aviation Forum*, 2020.

[9] Sjoerd Van Empelen and Roelof Vos. Effect of engine integration on a 4.6%-scale flying-v subsonic transport. In *AIAA Scitech 2021 Forum*.

[10] Jeroen van Uitert. Experimental investigation of flying v. Msc thesis, Delft University of Technology, Delft, The Netherlands, 2021.

[11] R.A. Viet. Analysis of the flight characteristics of a highly swept cranked flying wing by means of an experimental test. Master's thesis, Delft University of Technology, 2019.